JOURNAL OF THERMOPHYSICS AND HEAT TRANSFER
Vol. 16, No. 4, October–December 2002

Comparison of Surface Chemical Kinetic Models for Ablative Reentry of Graphite

Mark A. Havstad* and Robert M. Ferencz†
Lawrence Livermore National Laboratory, Livermore, California 94551

A general formulation for surface chemical reactions is used with a finite element heat conduction code to compare computations of the ablated mass flux from carbon bodies experiencing conditions representative of Earth reentry. Several credible models for the surface chemical kinetics are exercised with the formulation and are compared both to each other and to test data obtained by the Passive Nosetip Technology program in the mid-1970s. Sublimation of C_5 and C_7 is shown to be a concern for surface temperatures greater than about 3900 K. The best match between measurements and the calculations is obtained with surface chemical models that use the usual CO formation reactions and the sublimation of C_1–C_3 but that also include CN formation and the sublimation of C_5 and C_7. For surface temperatures above 3500 K and for similar assumptions for the equilibrium vapor pressure and evaporation coefficients of the sublimated species, the net reaction rate approach and the surface site occupation approach give similar ablated mass fluxes.

Nomenclature

B	=	surface atom site density, $1/m^2$
c	=	specific heat, J/kg · K
D	=	stoichiometry matrix
e	=	energy, J/kg
F	=	Gibbs free energy, J/gmol
F	=	radiation view factor
f	=	kinetic rate factor, $1/m^2s$ or nondimensional
H^0_{298}	=	enthalpy of formation at 298 K, J/gmol
h	=	enthalpy, J/kg
h	=	Planck's constant, J · s
k	=	Boltzmann's constant, J/molecule · K
k	=	reaction rate constant, $1/m^2s$
L	=	number of surface species
l	=	surface species index
M	=	molecular weight, kg/kmol
m	=	mass per molecule, kg
$\dot{m}$	=	mass flux, kg/m^2s
N_0	=	Avogadro's number, 1/kmol
P	=	pressure, N/m^2
P_0	=	reference pressure, atmosphere, 0.101325 MPa
p	=	pressure, N/m^2
Q	=	number of surface reactions
q	=	chemical species index
$\dot{q}$	=	heat flux, J/m^2s
R	=	linear correlation coefficient
R_u	=	universal gas constant, J/kmol · K or J/gmol · K
r	=	forward reaction rate, m^2s
S	=	surface kinetic factor, $1/m^2s$ or nondimensional
T	=	temperature, K
W	=	number of gaseous species
w	=	gaseous species index
X	=	mole fraction of gaseous species
γ	=	concentration, kmol/kg
ε	=	emissivity
ε	=	parameter in surface species reaction constant
η	=	stoichiometric coefficient of surface reactants
θ	=	surface species population fraction
λ	=	stoichiometric coefficient of surface products
μ	=	stoichiometric coefficient of gaseous products
ν	=	stoichiometric coefficient of gaseous reactants
σ	=	Stefan–Boltzmann constant, $J/m^2s \cdot K^4$
Φ	=	modification factor in heat transfer relation

Subscripts

a	=	activation
ab	=	ablation
abspec	=	ablated species
blow	=	blowing
cw	=	cold wall
diff	=	diffusion
emittradn	=	emitted radiation
eq	=	equilibrium
er	=	erosion
f	=	forward
f	=	formation
flcondn	=	fluid conduction
HAL	=	heating augmentation level
i	=	mass species index
incradn	=	incident radiation
k	=	element index
m	=	reaction index
p	=	pressure
pyrgas	=	pyrolysis gas
q	=	reaction index
r	=	recovery
ref	=	reference
reflradn	=	reflected radiation
s	=	species index
s,l	=	solid to liquid
solcondn	=	solid conduction
stag	=	stagnation
T	=	temperature
und	=	underside
u	=	universal
v	=	volume
w	=	wall
ν	=	vibrational

Received 19 November 2001; revision received 25 April 2002; accepted for publication 25 April 2002.

*Mechanical Engineer, New Technologies Engineering Division, P.O. Box 808, L-140. Member AIAA.

†Mechanical Engineer, Defense Technologies Engineering Division, P.O. Box 808, L-125. Senior Member AIAA.

Superscript

0 = formation

Introduction

ABLATION of graphite on atmospheric reentry continues to be actively studied, both to achieve greater fidelity of simulation and to support new concepts.[1,2] Despite the maturity of the field (key studies[3] date to at least 1965), models for the surface chemical kinetics differ from study to study. Keenan[4] and Keenan and Candler[5,6] modeled the surface chemistry with three oxidation reactions described by Park[7] and three sublimation reactions (C_1–C_3) with constants taken from the recommendations by Baker.[8] These sublimation constants appear largely to come from compilations due to Palmer and Shelef[9] and Palmer.[10] Park and Ahn[11] and Suzuki et al.[2] modeled graphitic reentry into Earth atmosphere using just one of the three oxidation reactions of Parks's[7] fundamental work, one sublimation reaction (C_3), one CN formation reaction, and an ion–electron recombination reaction. The constants for the C_3 sublimation reaction, attributed to a different study by Baker et al.,[12] give significantly lower sublimation for temperatures above 3000 K than would be given using the values from Keenan.[4] Zhluktov and Abe[13] used a more fundamental expression for the surface chemical kinetic effects. They arrived at a new set of constants for their more complex set of oxidation reactions and considered at least three different sources for the constants in the sublimation reactions. These sources were Baker,[8] Scala and Gilbert,[3] and Blottner.[14] Further, computations using the Apollo-era ACE phenomenological model continue to have wide use,[15–17] and curve fits to its results have been given in a review paper where heat balance integral calculations are used to estimate ablation of graphite on reentry.[18]

In each of these studies, the surface chemistry model was coupled to a particular fluid computational approach to generate a consistent solution. For clarity of comparison and simplicity, here we take the stagnation-point fluid solution from one of the studies[4] and use it without variation for generation of estimates of ablation and thermal response of a graphitic body with a variety of surface chemical kinetic models. The calculations have been done within a general-purpose finite element heat transfer code, TOPAZ3D,[19] with an implementation of the general heterogeneous chemical kinetics derived from Ref. 13. The ablative surface chemistry generates a nonlinear heat flux boundary condition applied to the surface facets modeling the exterior of the reentering body. This formulation allows rapid comparison of surface chemical systems and comparison to tests.[20,21]

Theory

Mass and energy balances for ablating materials were given in detail in Refs. 17, 18, and 22. For mass balance on a control volume of infinitesimal thickness centered on an ablating surface we have

$$\dot{m}_{\text{ab}} + \dot{m}_{\text{er}} + \dot{m}_{\text{pyrgas}} = \dot{m}_{\text{und}} + \dot{m}_{\text{pyrgas}} \tag{1}$$

Leaving the control volume on the fluid side are ablative, erosive, and pyrolysis gas terms. Entering the control volume from the opposite side are the pyrolysis gas and the solid material (which enters because the control volume must be receding into the solid to stay centered on the ablating surface). Only carbon–carbon or graphite aeroshells are considered here and so pyrolysis terms are eliminated. Furthermore, we ignore possible erosion because this behavior is poorly understood.

The energy balance equation for the same volume of infinitesimal thickness can be written

$$\dot{q}_{\text{flcondn}} + \dot{q}_{\text{diff}} + \dot{q}_{\text{incradn}} = \dot{q}_{\text{solcondn}} + \dot{q}_{\text{reflradn}} + \dot{q}_{\text{emittradn}} + \dot{q}_{\text{abspec}} \tag{2}$$

Terms on the left indicate heat input to the control volume from the fluid side. The first two terms, the heat diffusion and mass diffusion contributions, are generally supplied by a computational fluid dynamics (CFD) solution. The third term on the left is the incident radiation from the fluid side. On the right-hand side are terms for the conducted heat into the interior of the solid, reflected and then emitted radiation, and last the enthalpy carried out of the control volume by ablation products. This last term on the right-hand side includes both the enthalpy of the material ejected to the flowfield from the control volume and the enthalpy of the underside material moving into the control volume. The concentration of surface reacting species implied by this energy balance should be obtained consistent with a balance between the rate of production of species at the surface and the rate fluid reactant species diffuse to the surface; for example, see Ref. 4.

Combining the radiation terms, expressing the heat load from the fluid side as a function of the cold wall heat flux, and giving the ablative transport as a function of the mass flux and an enthalpy difference, one obtains

$$\dot{q}_{\text{solcondn}} = \dot{q}_{\text{cw}}(1 - h_w/h_r)\Phi_{\text{blow}}\Phi_{\text{HAL}} - \varepsilon\sigma\left(T_w^4 - T_{\text{ref}}^4\right) - \dot{m}_{\text{ab}}(h_w - h_{\text{und}}) \tag{3a}$$

$$\dot{q}_{\text{solcondn}} = \dot{q}_w^{\text{CFD}} - (1 - \alpha_w)q_{\text{incradn}} - F\sigma T_w^4 - \dot{m}_{\text{ab}}(h_w - h_{\text{und}}) \tag{3b}$$

Equation (3a) is given in the 1995 review by Potts[18] and Eq. (3b) is given in the 1994 review by Milos and Rasky.[17] The blowing constant is computed as in Refs. 17 and 18, and the heating augmentation level Φ_{HAL} is unity for clear air and nonerosive entry. The underside enthalpy is computed here as in Ref. 18, which roughly agrees (within 5%) with that used by Keenan.[4] The wall gas enthalpy is normally determined by the CFD solution, although for the aerotherm chemical equilibrium (ACE)-based calculations given in Ref. 18, there are also curve fits for h_w. Here the coupling to a CFD solution is not done. For the purpose of comparing only the surface chemical models, we have frozen the wall gas composition. (A single wall gas composition provides a uniform comparison between surface models.) We then consider a different control volume than that used for the mass and energy balances given earlier. As before, the inner control surface is infinitesimally displaced into the solid. However, instead of placing the outer control volume boundary infinitesimally displaced into the fluid from the ablating surface, it is placed on the aeroshell surface and recedes with it. The surface chemical reaction rate then determines a heat load:

$$\dot{q}_{\text{surf}} = \frac{1}{N_0}\sum_{s=1}^{\text{nspec}} M_s h_{f,s} \sum_{q=1}^{Q} D_{s,q} r_q \tag{4}$$

The enthalpy to form and destroy surface species, due to the net surface reaction rates, determines the ablative transport term (along with the underside enthalpy flux). Thus, the energy balance used here with the surface chemical kinetic calculations (not ACE based) is

$$\dot{q}_{\text{solcondn}} = \dot{q}_{\text{cw}}(1 - h_w/h_r)\Phi_{\text{blow}}\Phi_{\text{HAL}} - \varepsilon\sigma\left(T_w^4 - T_{\text{ref}}^4\right) - \dot{q}_{\text{surf}} + \dot{m}_{\text{ab}}h_{\text{und}} \tag{5}$$

This energy balance applies for a fixed-wall gas assumption. We choose to use a wall gas composition reported[4–6] for conditions of a 70-atm stagnation pressure and the Park[7]–Keenan–Candler[4–6] (PKC) surface chemical model described later. We then apply the balance and invariant wall gas composition for a range of pressures above and below 70 atm to further compare surface kinetic models. Calculations with variable wall gas compositions are in work. A generalized version of the surface chemistry formulation given by Zhluktov and Abe[13] was derived in Ref. 22:

$$r_q = k_{fq}\prod_{w=1}^{W}[PX_{qw}]^{\nu_{qw}}\prod_{l=1}^{L}\theta_l^{\eta_{ql}} - k_{rq}\prod_{w=1}^{W}[PX_{qw}]^{\mu_{qw}}\prod_{l=1}^{L}\theta_l^{\lambda_{ql}} \tag{6}$$

The two terms on the right give the rates that reaction q goes forward and backward, respectively. Just as with homogeneous chemical kinetics, the rate that reactions run forward depends on stoichiometry and availability of reactants, and the rate that they run backward

depends on stoichiometry and availability of products. Here, there are two product terms for each of the right-hand-side terms because the fluid species and the surface species are tracked separately. The forward and backward reaction rate constants, k_{fq} and k_{rq}, are specified from a combination of theory and experiments. The following expression for the forward reaction rate encompasses a number of prevalent forms[13]:

$$k_{fq} = \varepsilon_q f_q S_q e^{T_{aq}/T}$$
$$S_q = 1 \quad \text{or} \quad S_q = BkT/h$$
$$f_q = P_0 \Big/ \sqrt{2\pi m_i kT} \quad \text{or} \quad f_q = 1 \tag{7}$$

The S_q term allows for a surface site density B to affect the reaction rate. Backward reaction rate constants may also take this form. In this formulation there are L unknown surface concentrations and $4Q$ more unknowns, r_q, k_{rq}, k_{fq}, and K_q. The definition of the equilibrium constant, the reaction rate equations, and the relations for the reaction rate constants provide $3Q$ relations. Constraints on surface site occupation provide L relations.[22] Equilibrium constant data provide Q more relations. The JANAF tables[23] are one choice for these data, but simple relations are also available for some materials.

Sublimation reactions will be of particular importance here. Typically, sublimation is considered as driven by a difference between the equilibrium vapor pressure of species s and the actual vapor of s beside the surface. Thus, mass flux by sublimation is represented by a $(p_{\text{eq},s} - p_s)$ term or an equilibrium composition difference term $(\gamma_{\text{eq},s} - \gamma_s)$. Such relations, often referred to as Knudsen–Langmuir equations or Hertz–Knudsen–Langmuir equations, are a special case of the reaction rate equation (6), where the evaporation "reaction" runs forward at the rate given by the equilibrium vapor pressure, backward at the rate given by the pressure beside the surface, and the net rate is the difference between the two.

Within the bulk of the ablation literature to date, sublimation is typically handled by such a forward-minus-backward rate equation, but oxidation and other surface reactions are most often handled by net-reaction-rate equations, such as those given by Park.[7] With the current formulation the two can be mixed, or the fully reversible approach (with or without the surface occupation fractions θ_l^{ν} computed in Ref. 13) can be used. For any reaction to be specified as a net reaction rate, the equilibrium constant is set to be very large so that the backward reaction runs negligibly and the surface occupation stoichiometric coefficients are set to zero.

Sublimation of C_3 is central to determining mass loss from ablators above 3000 K; however, there is no agreement on the best set of basic parameters. With some manipulation it can be shown that Keenan,[4] Keenan and Candler,[5,6] Blottner,[14] Park and Ahn,[11] and Suzuki et al.[2] use the following relations for the equilibrium vapor pressure of C_3:

$$p_{\text{eq,Keenan},C_3} = 2.47 \times 10^{10} \times \exp[-93{,}227/T]$$
$$p_{\text{eq,Blottner},C_3} = 4.3 \times 10^{15} \times T^{1.5} \times \exp[-97{,}597/T]$$
$$p_{\text{eq,Park},C_3} = 1.56 \times 10^{5} \times \exp[-59{,}410/T] \tag{8}$$

Each of these expressions uses a constant term in the exponential, an approximation that the free energy of formation of the vapor is not a function of temperature. The free energy of formation (and thence the equilibrium vapor pressure) of carbon species C to C_7 has been computed from data and partition functions.[24,25] For species C_n one has

$$p_{\text{eq,free-energy},c_n} = \exp\left\{ -\frac{\left(F_T^0 - H_{298}^0\right)}{R_u T}\bigg|_{C_n} + \frac{n\left(F_T^0 - H_{298}^0\right)}{R_u T}\bigg|_{s/l} - \frac{\Delta H_{\text{RXN},298}^0}{R_u T} \right\} \tag{9}$$

The enthalpy of formation at 298 K is a constant, but both of the free energy terms are functions of temperature, as given in Refs. 24 and 25. The four preceding relations and the JANAF table data[23] for C_3 are plotted in Fig. 1. A recent report for a slender-body reentry[1] gave a peak temperature of roughly 4600 K, a range where discrepancies among the C_3 equilibrium computations shown are substantial.

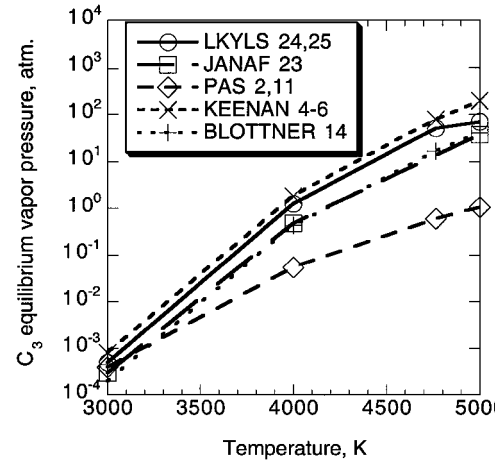

Fig. 1 Estimates of the equilibrium vapor pressure of C_3.

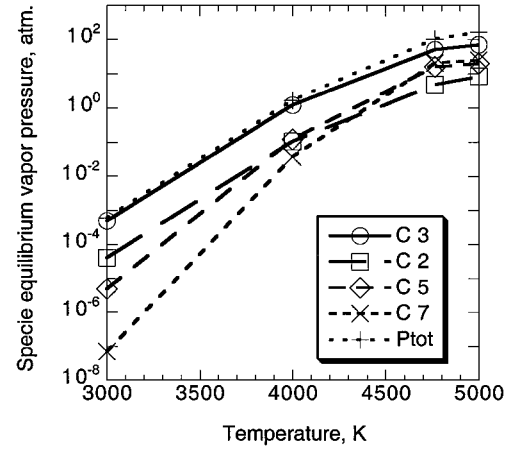

Fig. 2 Estimates of the equilibrium pressure of carbon species.

The possibility of 4600 K and higher temperatures also makes C_2, C_5, and C_7 candidates for significant contributions to ablative mass flux. The equilibrium vapor pressures of C_2, C_3, C_5, and C_7 and the total pressure as a function of temperature as computed by Leider et al.[24] and Lee and Sanborn[25] are given in Fig. 2. At 3000 K, C_3 is 82% of the total pressure; at 4000 K, 75%; and at 4765 K, 50%. In addition to potentially enhancing surface recession, the presence of these additional polyatomic carbon species would alter near-wall flow compositions by reacting with O and N and convecting additional C species downstream. Given these possible effects at higher tempatures, it would appear preferable to include these species in surface kinetic models and the allied flow simulations.

Surface Reactions

Park[7] described oxidation of graphite on reentry with three reactions (reaction set 1):

1) $(C) + O_2 \Rightarrow CO + O$
2) $(C) + O \Rightarrow CO$
3) $(C) + O + O \Rightarrow (C) + O_2$

Any item in parentheses is a surface species rather than a fluid species. Sublimation of surface C–C_7 is represented by the following (reaction set 2):

4) $(C) \Leftrightarrow (C) + C$
5) $2(C) \Leftrightarrow 2(C) + C_2$
6) $3(C) \Leftrightarrow 3(C) + C_3$
7) $4(C) \Leftrightarrow 4(C) + C_4$
8) $5(C) \Leftrightarrow 5(C) + C_5$
9) $6(C) \Leftrightarrow 6(C) + C_6$
10) $7(C) \Leftrightarrow 7(C) + C_7$

Table 1 Surface reactions and rate constants

Reaction	Model participant PKC	PKCH	PKCHF	ZA	$k_{f,q}$	$k_{r,q}$
1) $(C)+O_2 \Rightarrow CO+O$	×	×	×		$\frac{0.00143+0.01\exp(-1450/T)}{1+0.0002\exp(13{,}000/T)}$	0
2) $(C)+O \Rightarrow CO$	×	×	×		$0.63\exp\left(-\frac{1160}{T}\right)$	0
3) $(C)+O+O \Rightarrow (C)+O_2$	×	×	×		$0.63\exp\left(-\frac{1160}{T}\right)$	0
4) $(C) \Leftrightarrow (\,C\,)+C$	×	×	×		$\frac{0.14P_0}{(2\pi mkT)^{\frac{1}{2}}}$	$1.31\times10^{8}\times\exp\left(-\frac{85{,}715}{T}\right)$
5) $2(C) \Leftrightarrow 2(C)+C_2$	×	×	×		$\frac{0.26P_0}{(2\pi mkT)^{\frac{1}{2}}}$	$4.38\times10^{9}\times\exp\left(-\frac{98{,}363}{T}\right)$
6) $3(C) \Leftrightarrow 3(C)+C_3$	×	×	×		$\frac{0.03P_0}{(2\pi mkT)^{\frac{1}{2}}}$	$2.47\times10^{10}\times\exp\left(-\frac{93{,}227}{T}\right)$
7) $N+(C) \Rightarrow CN$		×	×		$\frac{P_0}{(2\pi mkT)^{\frac{1}{2}}}$	0
8) $5(C) \Leftrightarrow 5(C)+C_5$			×		$\frac{0.015P_0}{(2\pi mkT)^{\frac{1}{2}}}$	$4.54\times10^{12}\times T^{-0.266}\times\exp\left(-\frac{117{,}049}{T}\right)$
9) $7(C) \Leftrightarrow 7(C)+C_7$			×		$\frac{0.015P_0}{(2\pi mkT)^{\frac{1}{2}}}$	$6.68\times10^{12}\times T^{0.504}\times\exp\left(-\frac{149{,}439}{T}\right)$
10) $O+(C) \Leftrightarrow (C-O)$				×	$\frac{P_0}{(2\pi mkT)^{\frac{1}{2}}}$	$\left[\frac{BkT}{P_0}\left(\frac{2\pi mkT}{h^2}\right)^{\frac{1}{2}}\exp\left(-\frac{45{,}000}{T}\right)\right]^{-1}k_{f,10}$
11) $O_2+2(C) \Leftrightarrow 2(C-O)$				×	$\frac{0.0008P_0}{(2\pi mkT)^{\frac{1}{2}}}B\frac{kT}{h}\exp\left(-\frac{30{,}800}{T}\right)$	JANAF[23] data and $k_{r,10}$[a]
12) $O_2+(C) \Leftrightarrow (C-O)+O$				×	$\frac{P_0}{(2\pi mkT)^{\frac{1}{2}}}\exp\left(-\frac{14{,}200}{T}\right)$	JANAF[23] data and $k_{r,10}$[a]
13) $CO_2+(C) \Leftrightarrow (C-O)+CO$				×	$\frac{0.9P_0}{(2\pi mkT)^{\frac{1}{2}}}$	JANAF[23] data and $k_{r,10}$[a]
14) $(C-O) \Leftrightarrow CO+(C)$				×	$\frac{0.1P_0}{(2\pi mkT)^{\frac{1}{2}}}B\frac{kT}{h}\exp\left(-\frac{40{,}000}{T}\right)$	JANAF[23] data, $k_{r,17}$, and $k_{r,10}$[a]
15) $O+(C-O) \Leftrightarrow CO_2+(C)$				×	$\frac{0.8P_0}{(2\pi mkT)^{\frac{1}{2}}}\exp\left(-\frac{2000}{T}\right)$	JANAF[23] data, $k_{r,17}$, and $k_{r,10}$[a]
16) $2(C-O) \Leftrightarrow CO_2+2(C)$				×	$\frac{P_0}{(2\pi mkT)^{\frac{1}{2}}}B\frac{kT}{h}\exp\left(-\frac{40{,}000}{T}\right)$	JANAF[23] data, $k_{r,17}$, and $k_{r,10}$[a]
17) $(C) \Leftrightarrow (C)+C$				×	$\frac{0.24P_0}{(2\pi mkT)^{\frac{1}{2}}}$	$9.30\times10^{7}\times\exp\left(-\frac{85{,}334}{T}\right)$
18) $2(C) \Leftrightarrow 2(C)+C_2$				×	$\frac{0.50P_0}{(2\pi mkT)^{\frac{1}{2}}}$	JANAF[23] data and $k_{r,17}$[a]
19) $3(C) \Leftrightarrow 3(C)+C_3$				×	$\frac{0.023P_0}{(2\pi mkT)^{\frac{1}{2}}}$	JANAF[23] data and $k_{r,17}$[a]
20) $N+(C) \Leftrightarrow (C-N)$				×	$\frac{P_0}{(2\pi mkT)^{\frac{1}{2}}}$	$\left[\frac{BkT}{P_0}\left(\frac{2\pi mkT}{h^2}\right)^{\frac{1}{2}}\exp\left(-\frac{36{,}600}{T}\right)\right]^{-1}k_{f,20}$
21) $(C-N)+N \Leftrightarrow N_2+(C)$				×	$\frac{P_0}{(2\pi mkT)^{\frac{1}{2}}}\exp\left(-\frac{76{,}600}{T}\right)$	JANAF[23] data and $k_{r,20}$[a]

[a]See Ref. 13.

Because of the macroscopic thickness of typical substrates, surface C species do not deplete: If a C leaves, then another appears from below, albeit possibly leaving the surface rougher. The reappearance of C at sites that lose a C explains why the sublimation reactions above can fail to "balance" on an elemental basis. Note that reaction set 1 is a set of net rate reactions and this is denoted by the right-facing arrow in each of the reaction definitions. In contrast, reaction set 2 describes reactions that run forward and backward and the arrow symbol in the seven reactions is bidirectional. This convention is used in the subsequent text and Table 1.

The nitrogen reaction given by Park and Ahn[11] is as follows (reaction set 3):

11) $N + (C) \Rightarrow CN$

Graphite oxidation reactions given by Zhluktov and Abe[13] are represented by the following (reaction set 4):

12) $O + (C) \Leftrightarrow (C - O)$
13) $O_2 + 2(C) \Leftrightarrow 2(C - O)$
14) $O_2 + (C) \Leftrightarrow (C - O) + O$
15) $CO_2 + (C) \Leftrightarrow (C - O) + CO$
16) $(C - O) \Leftrightarrow CO + (C)$
17) $O + (C - O) \Leftrightarrow CO_2 + (C)$
18) $2(C - O) \Leftrightarrow CO_2 + 2(C)$

Nitrogen reactions given by Zhluktov and Abe[13] are as follows (reaction set 5):

19) $N + (C) \Leftrightarrow (C - N)$
20) $(C - N) + N \Leftrightarrow N_2 + (C)$

Combinations of reactions 12–18 have a similar net effect as reactions 1–3. For example, reactions 12–15, when they run forward, describe putting O atoms on the surface (adsorption). Reaction 16, when going forward, describes the release of the formed surface C–O complex to the gas phase. Reactions 1 and 2 describe CO release, one by splitting O_2, the other by reaction with atomic O. Reactions 19 and 20 describe cyanogen formation and nitrogen desorption, respectively. The associated mathematics for the net reaction rate equations (reactions 1–3 and 11) is decidedly simpler than that considering surface complex formation. However, asserting that there are a finite number of sites at which only a single process can occur at any time (e.g., a site cannot sublimate while it is occupied with O) is a physically reasonable constraint.

Of course more complex sets of reactions can be specified, but the bulk of the recent work in surface kinetics of ablative reentry is formed from these reactions. Reactions 1–6 comprise the entirety of the surface model PKC in Refs. 4–6. Reactions 4–6 and 12–20 are the surface model of Zhluktov and Abe[13] (ZA). In Refs. 2 and 11, the surface model is simplified to reactions 2, 6, and 11 and an electron–ion recombination reaction, which we ignore here because it has no direct effect on net mass flux. The surface chemical models used here are summarized in Table 1.

For each time step of a thermal calculation using a surface chemical model there is a system of ordinary differential equations to be solved for every ablating facet. A fast and stable solver, DVODE,[26] is used to obtain the local surface species concentrations and the reaction rates, which then give the local heat load to the solid. Thus, at each time step the conduction equation is resolved until the temperature-dependent heat load converges.

Tests and Models

Despite the large number of experimental ablation studies in the open literature, many done with varying types of graphite, few were reported with sufficient detail to be reproduced. The more extensive efforts were probably those reported by Maahs,[27] Baker et al.,[28] and Lundell and Dickey[29] and the Passive Nosetip Technology (PANT) program.[20,21] The PANT reports are unique in that they give freestream conditions and then present stagnation-point recession and temperature as a function of stagnation-point pressure from less than 10 up to 250 atm. A variety of graphite plugs and cones were tested in arc jet and ballistic range facilities. In many tests, reasonably steady recession rates are shown for test times on the order of 4–30 s.

The PANT results (and power law curve fits) for stagnation-point temperature and ablative mass flux are given in Figs. 3–5. The experimental uncertainty of the individual points were never documented, but given the variety and number of the tests, test facilities, model sizes, and model shapes, the scatter in the plotted results is not extreme. Perhaps the principal shortcoming of the work is the paucity of mass flux data below 80 atm.

A range of ATS-J graphite geometries were tested in the PANT program, but a reasonable approximation to many of the samples is the plug shape selected by Keenan[4]: a cylinder of ~15.0-mm length and 6.35-mm diam capped at the flow-facing end with a hemisphere.

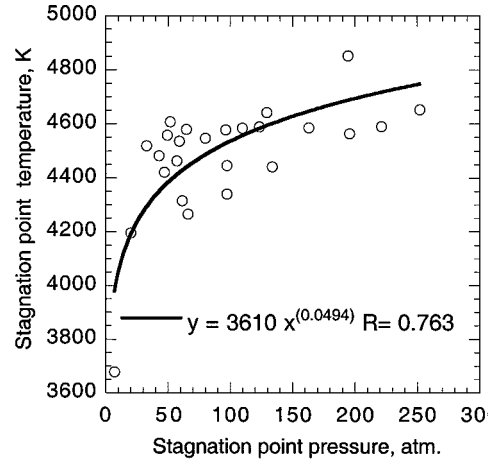

Fig. 3 Stagnation-point temperatures measured in PANT test sequence and a power law fit to these data.

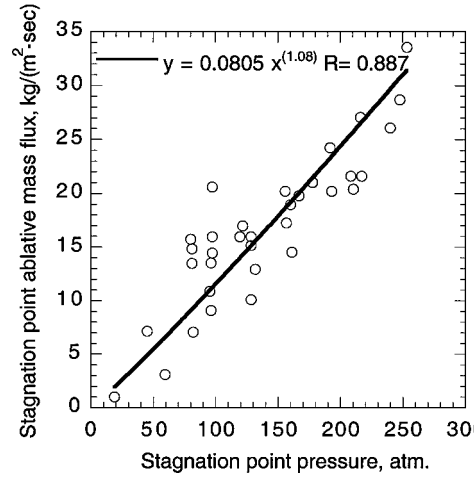

Fig. 4 Stagnation-point mass fluxes measured in PANT test sequence.

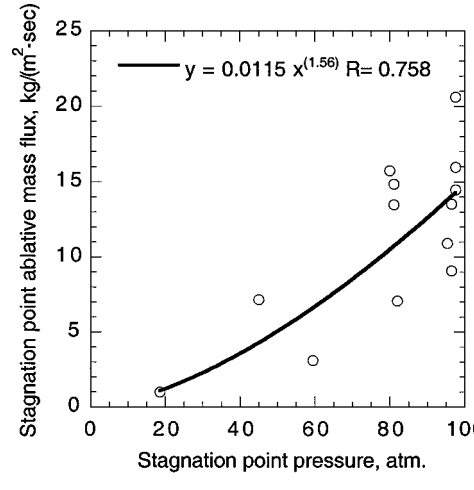

Fig. 5 Stagnation-point mass fluxes for stagnation-point pressures less than 100 atm measured in PANT test sequence.

In the comparisons to be reported, this geometry and an expanded representation of the stagnation point (in effect a one dimensional stagnation-point model) are used with combinations of the surface chemical reactions given earlier. A combination of the relations given by Potts[18] and Havstad and Carter[22] are used for the material properties, aerodynamic heating, and stagnation-point pressure. For the fully three-dimensional modeling, the stagnation pressure on the surface of the body varies with the cosine squared over the first 80 deg of the hemisphere and constant over the rest of the body. For the aerodynamic heating, a cosine dependence is used to 80 deg. The flats on the rear of the models were adiabatic, and the remainder of the exterior surfaces were ablative, depending on local temperature, as given by the energy balances given earlier. Calculations were executed in the transient mode until approximate steady state was reached. Computations invoking the ACE-based curve fits[18] matched those given in Ref. 22, and those using the surface chemical kinetics models used gas compositions at the wall taken from Keenan.[4] Using a fixed-wall gas composition is not fully physically consistent, particularly at the extremes of stagnation pressures simulated here, but has the advantage of temporarily eliminating the coupling between the CFD solution and the surface chemistry. The results then compare surface chemical activity and mass flux for identical wall gas compositions: Discrepancies are due solely to the surface chemical kinetic model operative and not to any variation of coupling (however physically reasonable it is) between the ablation and the reactive flow physics. The blowing correction does vary with the ablative mass flux here. The wall gas composition used was obtained from a balance of diffusion to the wall and surface production rate for a single surface model (PKC) and set of freestream conditions (70-atm stagnation pressure) in Ref. 4. Further discussion of the fixed-wall gas assumption is given in the "Results" section.

Results

The variations of stagnation-point temperature with stagnation-point pressure for six sets of calculations and also experimental data are given in Fig. 6. The PANT points are derived from a power law fit to the PANT program data plotted in Fig. 3:

$$T = 3613 \times P_{\text{stag}}^{0.049418}, \qquad R = 0.763 \tag{10}$$

The Keenan points are numerical results from Ref. 4. The ACE points were computed in TOPAZ3D using the curve fits to the ACE program generated in Ref. 18 and most of the rest of the methodology therein. The PKC points were computed using the model employed by Keenan and Candler[4–6] that relies on the oxidation work of Park.[7] The ZA points used the model given by Zhluktov and Abe[13] with the sublimation parameters given in the 1977 publication of Baker.[8] The PKCH results were computed using an enhanced version of the above PKC model: CN formation is included as given in Ref. 11. The PKCHF results were generated by enhancing the

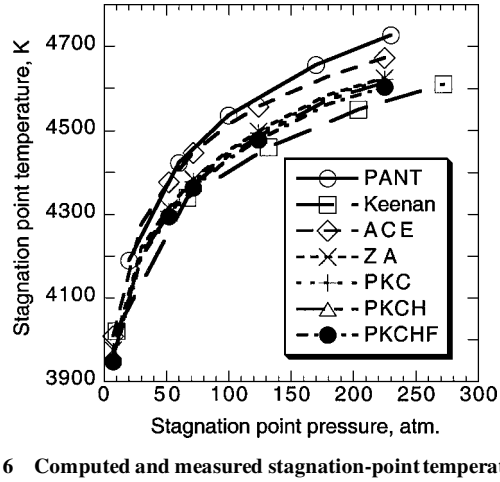

Fig. 6 Computed and measured stagnation-point temperatures.

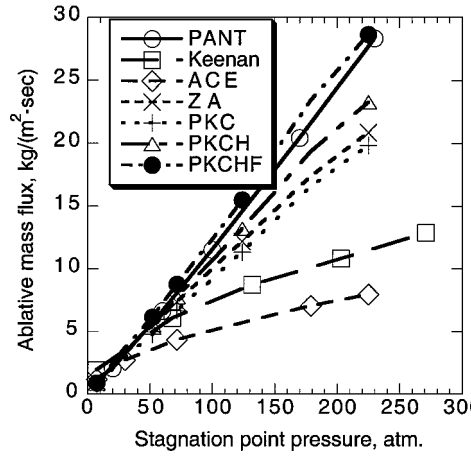

Fig. 7 Computed and measured stagnation-point mass fluxes.

PKCH model with fits to the C_5 and C_7 sublimation information given in Refs. 24 and 25:

$$p_{\text{eq},LKYLS,C_5} = 2.405 \times 10^{12} \times T^{-0.161} \exp(-117{,}783/T)$$

$$p_{\text{eq},LKYLS,C_7} = 6.838 \times 10^{12} \times T^{0.555} \exp(-150{,}932/T) \tag{11}$$

with a vaporization constant $\varepsilon = 0.015$ for both. This value is the lowest of the values used for C_1–C_3. Given the large body of literature on laser ablation of carbon for thin-film growth, it is likely that fairly well-supported values of ε for C_5 and C_7 can be deduced.

The results for temperature are best interpreted by also referring to the stagnation-point mass flux (Fig. 7). For example, the ACE-based calculations most closely match the PANT temperature data, but they do so with the least mass flux, that is, the least reduction in aerodynamic heating from blowing into the boundary layer. In contrast, the PKCH temperatures are lower than PKC values and PKCHF lower than PKCH because the added mass flux provided by each enhanced model increases the ablative blowing.

The PKC and Keenan[4] curves show good agreement for both mass flux and temperature near a stagnation-point pressure of ~70 atm, as they should because the PKC model was used in the calculations of Ref. 4 and the wall gas compositions at a stagnation pressure of 70 atm are used in the calculations here. The slight discrepancy between the Keenan[4] points and the PKC points at this pressure in Fig. 7 is reasonable given that the fluid species mass fractions were read from figures in Ref. 4. The increasing discrepancy between the Keenan and PKC points as one moves away from this pressure is also reasonable given that the fluid species mass fractions are not adjusting to the changes in surface production rates. For a coupled ablation–CFD computation, the mass fractions of the sublimating species in the fluid stream would rise as wall temperature rises and, thus, moderate the rapid rise in mass flux shown for pressures greater than 70 atm. The agreement between the ZA and PKC calculations is noteworthy. The ZA calculations depend on surface occupation fractions (as derived in Ref. 13) but the PKC calculations do not. Thus, ZA and PKC, despite being computationally diverse, are actually equivalent in the 3900 K and greater temperature range. Because they share the use of the Palmer and Shelef[9] carbon sublimation data, they give nearly the same answer for mass flux and surface recession over the majority of the range for which ablation is appreciable: two-thirds of the surface recession on reentry occurs above 3900 K in Ref. 18. This highlights the shortcoming in the PANT data set. It would have been preferable to have measurements at lower wall temperatures than are shown here (Fig. 1), but the requirement of steady-state test conditions makes only very low pressures capable of yielding temperatures below 3900 K. It is only by having transient conditions on actual reentry that one obtains wall temperatures of 2500–3900 K at reasonable pressures. To fully test the oxidation parameters in Ref. 13 requires ablation measurements in this lower temperature regime, where sublimation is not dominant.

The PKCH and PKCHF models provide substantially better matches to the mass flux test data over the higher stagnation pressure

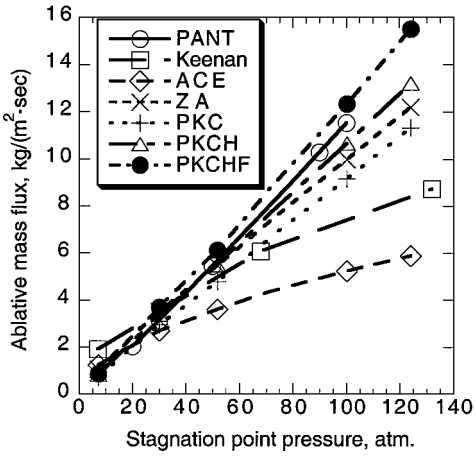

Fig. 8 Computed and measured stagnation-point mass fluxes limited to stagnation point pressures less than 140 atm.

range. If a fully coupled CFD–material response calculation had been done, these mass fluxes would be reduced somewhat but still greater than for any of the other models. Agreement or lack thereof in this range is worth examining. Stagnation pressures above 80 atm and mass fluxes above 10 kg/(m^2 · s) may not be applicable to any known or planned flight, but surface temperatures above 4400 K may be reasonable.[1] Whether transient or steady, such a surface temperature implies sublimation-driven mass transfer. The best estimates for equilibrium vapor pressure and thence sublimation are derived from the free energy calculations of Leider et al.[24] and Lee and Sanborn[25]: The experimental work of Baker et al.[12,28] is best interpreted with these calculations rather than JANAF data.[23] One alternate view is that the PANT data at elevated stagnation pressures involve mass transfer augmented by erosive action. There have been observations of particulate or erosive mass flux at elevated pressures.[30] However, analysis of the PANT data does not support a secondary and enhancing mechanism for mass loss. The power law fitted to the full data set is

$$\dot{m} = 0.08050 \times P_{\text{stag}}^{1.0782}, \qquad R = 0.887 \tag{12}$$

A similar fit to the subset with pressures less than 100 atm gives a much larger exponent:

$$\dot{m} = 0.01148 \times P_{\text{stag}}^{1.5559}, \qquad R = 0.758 \tag{13}$$

If erosion becomes operative at pressures above 100 atm, and other mechanisms hold steady, then the exponent on the power fit ought to grow rather than shrink as one progresses to higher pressures. Similarly, casual visual observation of Fig. 4 does not indicate a stagnation pressure where mass flux changes slope discontinuously. The simplest interpretation of the PANT data is that C_5 and C_7 sublimation contributes at elevated temperatures as predicted by theory[24,25] and supporting tests.[12,28] Unfortunately, use of $\varepsilon = 0.015$ for the C_5 and C_7 vaporization coefficients has not been fully justified yet.

The lower-half of the stagnation pressure range examined thus far is also of interest (Fig. 8). The level of agreement between the Keenan[4] calculation and the PKC and ZA models used here is more apparent in Fig. 8. For the 5–30-atm range all of the surface kinetic calculations performed here may be adequate. The PKC model slightly underpredicts mass flux relative to the PANT fit whereas the PKCHF model modestly overpredicts.

Conclusions

For surface temperatures above 3900 K, the surface occupation[13] and net reaction rate[2,4–6,11] surface kinetic formulations predict similar levels of ablative mass flux. Of the simple equations commonly used to represent the equilibrium vapor pressure of C_3 those given by Keenan[4–6] and Blottner[14] are preferred. Including CN gas formation by surface reaction contributes significantly to ablative mass flux over the elevated temperature range of 3900–4700 K. PANT test data for ablative mass flux are best matched by surface chemical kinetic models that approximate the equilibrium vapor pressure results of Leider et al.[24] and Lee and Sanborn.[25] including C_3, C_5, and C_7 terms.

Acknowledgment

This work was performed under the auspices of the U.S. Department of Energy by the University of California, Lawrence Livermore National Laboratory, under Contract W-7405-Eng-48.

References

[1] Kuntz, D. W., Hassan, B., and Potter, D. L., "Predictions of Ablating Hypersonic Vehicles Using an Iterative Coupled Fluid/Thermal Approach," *Journal of Thermophysics and Heat Transfer*, Vol. 15, No. 2, 2001, pp. 129–139.

[2] Suzuki, T., Furudate, M., and Sawada, K., "Unified Calculation of Hypersonic Flowfield for a Reentry Vehicle," AIAA Paper 2001-0980, Jan. 2001.

[3] Scala, S. M., and Gilbert, L. M., "Sublimation of Graphite at Hypersonic Speeds," *AIAA Journal*, Vol. 5 , No. 9, 1965, pp. 1635–1644.

[4] Keenan, J. A., "Thermo-Chemical Ablation of Heat Shields Under Earth Re-Entry Conditions," Ph.D. Dissertation, Dept. of Mechanical and Aerospace Engineering, North Carolina State Univ., Raleigh, NC, 1994.

[5] Keenan, J. A., and Candler, G. V., "Simulation of Ablation in Earth Atmospheric Entry," AIAA Paper 93-2789, July 1993.

[6] Keenan, J. A., and Candler, G. V., "Simulation of Graphite Sublimation and Oxidation Under Reentry Conditions," AIAA Paper 94-2083, June 1994.

[7] Park, C., "Effects of Atomic Oxygen on Graphite Ablation," *AIAA Journal*, Vol. 14, No. 11, 1976, pp. 1640–1642.

[8] Baker, R. L., "Graphite Sublimation Chemistry Nonequilibrium Effects," *AIAA Journal*, Vol. 15, No. 10, 1977, pp. 1391–1397.

[9] Palmer, H. B., and Shelef, M., "Vaporization of Carbon," *Chemistry and Physics of Carbon*, Vol. 4, Marcel Dekker, New York, 1968, pp. 85–135.

[10] Palmer, H. B., "On the Equilibrium Vapor Pressure of Graphite and the Temperature of the Carbon Arc," *Carbon*, Vol. 8, No. 2, 1970, pp. 243, 244.

[11] Park, C., and Ahn, H.-K., "Stagnation-Point Heat Transfer Rates for Pioneer-Venus Probes," *Journal of Thermophysics and Heat Transfer*, Vol. 13, No. 1, 1999, pp. 33–40.

[12] Baker, R. L., McDonough, J. M., Herr, K. C., Klingberg, R. A., Coffer, J. C., and Covington, M. A., "Carbon Vaporization Condensation Effects," NASA TM 87430, July 1984.

[13] Zhluktov, S. V., and Abe, T., "Viscous Shock-Layer Simulation of Airflow past Ablating Blunt Body with Carbon Surface," *Journal of Thermophysics and Heat Transfer*, Vol. 13, No. 1, 1999, pp. 50–59.

[14] Blottner, F. G., "Prediction of Electron Density in the Boundary Layer on Entry Vehicles with Ablation," *Entry Plasma Sheath and Its Effects on Space Vehicle Electromagnetic Systems*, NASA SP-252, Vol. 1, 1970, pp. 219–240.

[15] Hassan, B., Kuntz, D. W., and Potter, D. L., "Coupled Fluid/Thermal Prediction of Ablating Hypersonic Vehicles," AIAA Paper 98-0168, Jan. 1998.

[16] Chen, Y.-K., and Milos, F. S., "Two-Dimensional Implicit Thermal Response and Ablation Program for Charring Materials on Hypersonic Space Vehicles," AIAA Paper 2000-0206, Jan. 2000.

[17] Milos, F. S., and Rasky, D. J., "Review of Numerical Procedures for Computational Surface Thermochemistry," *Journal of Thermophysics and Heat Transfer*, Vol. 8, No. 1, 1994, pp. 24–34.

[18] Potts, R. L., "Application of Integral Methods to Ablation Charring Erosion, A Review," *Journal of Spacecraft and Rockets*, Vol. 32, No. 2, 1995, pp. 200–209.

[19] Shapiro, A. B., "TOPAZ3D—A Three Dimensional Finite Element Heat Transfer Code," Univ. of California, Rept. UCID-20484, Lawrence Livermore National Lab., Livermore, CA, 1985.

[20] Wool, M. R., "Passive Nosetip Technology (PANT) Program," ACUREX Corp., Final Summary Rept., AD-A019 186, SAMSO-TR-75-220, Los Angeles, June 1975.

[21] Shimizu, A. B., Ferrell, J. E., and Powars, C. A., "Passive Nosetip Technology (PANT) Program," Vol. 12, *Nosetip Transition and Shape Change Tests in the AFFDL 50 MW Rent Arc*, ACUREX Corp., Data Rept. AD-A020 710, SAMSO-TR-74-86, Los Angeles, April 1974.

[22] Havstad, M. A., and Carter, P., "Thermochemical Ablation During Reentrant and High Altitude Skipping Flight," AIAA Paper 2001-0979, Jan. 2001.

[23] Chase, M. W., "NIST–JANAF Thermochemical Tables, Fourth Edition," *Journal of Physical and Chemical Reference Data*, Monograph 9, Vols. 1, 2, 1998, pp. 550–1745.

[24]Leider, H. R., Krikorian, O. H., and Young, D. A., "Thermodynamic Properties of Carbon up to the Critical Point," *Carbon*, Vol. 11, No. 5, 1973, pp. 555–563.

[25]Lee, E. L., and Sanborn, R. H., "Extended and Improved Thermal Functions for the Gaseous Carbon Species C_1 to C_7 from 298 to 10000 K," *High Temperature Science*, Vol. 5, No. 6, 1973, pp. 438–453.

[26]Brown, P. N., Byrne, G. D., and Hindmarsh, A. C., "VODE, A Variable Coefficient ODE Solver," Lawrence Livermore National Lab., Univ. of California, Rept. UCRL-98412, Livermore, CA, June 1988.

[27]Maahs, H. G., "Ablation Performance of Glasslike Carbons Pyrolytic Graphite, and Artificial Graphite in the Stagnaton Pressure Range 0.035 to 15 Atmospheres," NASA TN D-7005, March 1972.

[28]Baker, R. L., Covington, M. A., and Rosenblatt, G. M., "The Determination of Carbon Thermochemical Properties by Laser Vaporization," *High Temperature Materials Chemistry Symposium*, Electrochemical Society, Pennington, NJ, 1983, pp. 143–154.

[29]Lundell, J. H., and Dickey, R. R., "Ablation of ATJ Graphite at High Temperature," *AIAA Journal*, Vol. 11, No. 2, 1973, pp. 216–222.

[30]Park, C., "Stagnation-Point Ablation of Carbonaceous Flat Disks, Part 2: Experiment," *AIAA Journal*, Vol. 21, No. 12, 1983, pp. 1748–1754.